Springer

KSME

Journal of Mechanical Science and Technology 31 (3) (2017) 1213~1222
www.springerlink.com/content/1738-494x(Print)/1976-3824(Online)
DOI 10.1007/s12206-017-0220-3

The characteristics investigation under the unsteady cavitation condition in a centrifugal pump †

Jiaxing Lu[1], Shouqi Yuan[1,*], Parameswaran Siva[2], Jianping Yuan[1], Xudong Ren[3] and Banglun Zhou[1]

[1]*National Research Centre of Pumps, Jiangsu University, Zhenjiang, 212013, China*
[2]*Department of Mechanical Engineering, Texas Tech University, Lubbock, 79409, USA*
[3]*School of Mechanical Engineering, Jiangsu University, Zhenjiang, 212013, China*

(Manuscript Received June 22, 2016; Revised September 2, 2016; Accepted October 18, 2016)

Abstract

Numerical simulation and experimental method are combined to investigate the pump inlet and outlet pressure fluctuations, the vibration characteristics and the internal flow instabilities under the unsteady cavitation condition in a centrifugal pump. It is found that the unsteady cavitation starts to generate as the *NPSH*a is lower than 5.93 m. Apparent asymmetric and uneven cavity volume distribution on each blade and in the impeller can be observed as the *NPSH*a decreases from 4.39 m to 1.44 m, which includes the cavitation develops from cavitation surge, rotating cavitation to asymmetric cavitation. The flow vortexes in each blade channel are produced in the cavity trailing edges by the shedding and collapse of cavitation, which interfere with each other and aggravate the flow instabilities. The dominant frequencies of the pump inlet and outlet pressure fluctuations are the shaft frequency and blade passing frequency under the unsteady cavitation conditions, respectively. Broadband pulses are obtained from both the pump inlet and outlet pressure pulsations, which results from the random shedding and collapse of unsteady cavitation bubbles. Obvious corresponding relationship between the root mean squares of the vibration measured in different positions and the suction performance curve is found under both the non-cavitation and unsteady cavitation conditions.

Keywords: Centrifugal pump; Unsteady cavitation; Experiment; Vibration; Pressure pulsations

1. Introduction

Inception of cavitation occurs as the pressure in the liquid is lower than the saturated vapor pressure of that liquid at a specific temperature [1]. Usually, cavitation is a complicated phenomenon in hydraulic machineries, which gives rise to great harm to the system. Most hydraulic machineries including turbines, pumps, turbo-pump inducers, hydrofoils, and propellers etc. are suffered from cavitation [2, 3]. Cavitation can not only produce the vibration, noise of the system and the instabilities of the inner flow, but also be responsible for the sharp decrease of efficiency in pumps, and even for the erosive damage on the surface of flow channels [4-11]. It is found that the cavitation instabilities occur when a turbulent flow interacts with the leading edge of the next blade, which leads to the high dynamic pressure fluctuations on the blades in pumps [12]. With the decreasing of pump inlet pressure, the cavitation process in a centrifugal pump includes the incipient cavitation, in which the vapor bubbles are generating near the leading edge [13]; quasi-steady cavitation, which is the condition between the incipient cavitation and unsteady cavitation in a centrifugal pump [14, 15]; and unsteady cavitation, in which the noise and vibration are induced [16]. Many types of cavitation instabilities in inducer have been presented, which mainly include Asymmetric cavitation (AC), Rotating cavitation (RC), Cavitation surge (CS), and high-order instabilities [17, 18]. Based on these cavitation instabilities mentioned above, Asymmetric cavitation (AC) with uneven cavity lengths is often observed in inducers at relatively low cavitation number [17, 19], which is an important unstable cavitation process and known as a source of shaft vibration induced by cavitation in turbomachinery [20]. The relationship between the unevenness of cavity length, unsteady fluid force, and the increase of shaft vibration in a cavitating inducer are discussed in Yoshida's research [21]. It is observed that the asymmetric cavitation pattern moves irregularly at the transition point from asymmetric cavitation to other types of cavitation instabilities [22]. The phenomenon that a large cavitating region rotate slower or faster than the rotator's speed is defined as subsynchronous RC or supersynchronous RC [23]. Cavitation surge (CS) and vortical flows in a diffuser with swirling flow is investigated by Ji et al. The underlying mechanisms of the interactions between the cavitation and the

*Corresponding author. Tel.: +86 511 88780007, Fax.: +86 511 88791739
E-mail address: shouqiy@ujs.edu.cn
† Recommended by Associate Editor Sangyoup Lee

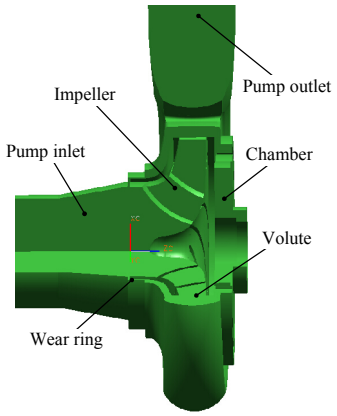

Fig. 1. Model for entire pump passage.

vortices is revealed [24]. Yoshida et al. find that Cavitation surge (CS) presents a low-frequency oscillation induced by the coupling of the cavitating rotator and the system, which needs to be avoided [25]. Tsujimoto et al. present that the cavitation instabilities occur if the steady cavity length becomes larger than about 65 % of the blade spacing [26]. Usually, strong force in the radial direction and vibration are produced by cavitation instabilities. Therefore, it is significant to do research about the unsteady cavitation in hydraulic machineries.

In order to improve the reliabilities of pump system, cavitation instabilities in centrifugal pumps should be put under control. In this paper, we primarily focus on the characteristics of the unsteady cavitation in a centrifugal pump. The relationship between cavity distribution and flow instabilities in the impeller are numerically presented. The inlet and outlet pressure pulsations of the pump under such conditions have been investigated through experimental method. At the same time, the relationship between the vibration and the development of cavitation in the pump has also been discussed.

2. Numerical method

The centrifugal pump studied in this research consists of a single suction, a spiral volute casing and a shrouded impeller with six blades. The designed rotating speed of the impeller is 2910 r/min. Therefore, the impeller blade passing frequency f_d and shaft frequency f_0 are around 291 Hz and 48.5 Hz, respectively. The designed head H and flow rate Q_d of the pump are 20.2 m and 50.6 m^3/h, respectively. According to the equation of the specific speed of the pump ($n_s = 3.65\ nQ^{0.5}/H^{0.75}$), the pump's specific speed is n_s = 132.2 at the designed point. More detailed geometry parameters of the pump are given in previous research [27, 28].

In order to take leakage flow effects into consideration, the volute and the side chambers between the impeller and the volute are included in the computational model in this study, shown in Fig. 1. The structured grids of the computational regions are generated by the ICEM CFD for the simulation. The grids in the tongue region and the boundary layer in all the domains are taken into concentrated, shown in Fig. 2. The

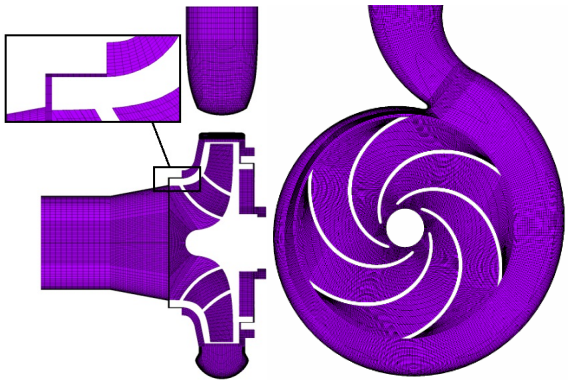

Fig. 2. Mesh for calculation.

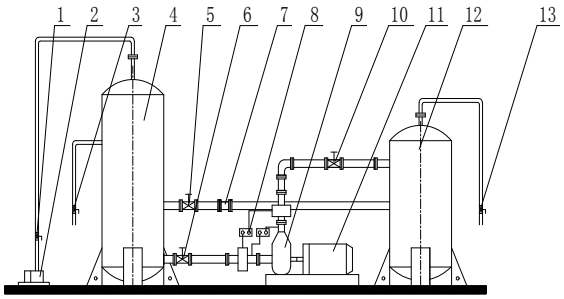

1, 3, 13. Ball valve; 2. Vacuum pump; 4. Pressure tank; 5, 10. Butterfly valve; 6. Gate valve; 7. Turbine flowmeter; 8. Pressure transmitter; 9. Test pump; 11. Electromotor; 12. Buffer tank.

Fig. 3. Schematic of the experimental test rig [27].

quality of the grids can meet the calculating requirements. The import and export of the pipe conduits are extended appropriately to render the numerical simulation more closing to the real situation. The commercial software ANSYS-CFX 14.5 is selected to do the calculation in the present study, and the k-ε model is chosen as turbulent model. The boundary conditions of the steady flow simulation are almost the same under both cavitation and non-cavitation conditions. The total pressure at the pump inlet is given, while mass flow rate is set as the outlet boundary condition.

3. Experimental method

The numerical results are validated by the measurements of pump performance. The pressure pulsations at the pump inlet and outlet are tested during the development of cavitation. Meanwhile, the vibration signals in different positions are also obtained as the cavitation progressed. As depicted in Fig. 3, the experiments are carried out in a closed hydraulic test rig. The stereogram of the rig and the positions of the apparatuses are shown in Fig. 4. During the experiment, the flow rate is measured by a turbine flow meter installed at the downstream pipe. The mean static pressure is tested by two pressure transmitters with the ranges from 0 to 4 bar installed at the outlet of the pump and -1 to 0.6 bar mounted at the inlet of the pump. Two transient pressure sensors with the ranges of -100

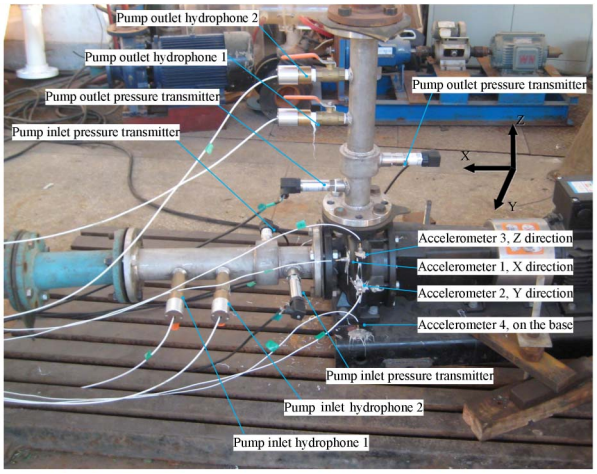

Fig. 4. Experimental set up with instrumentation.

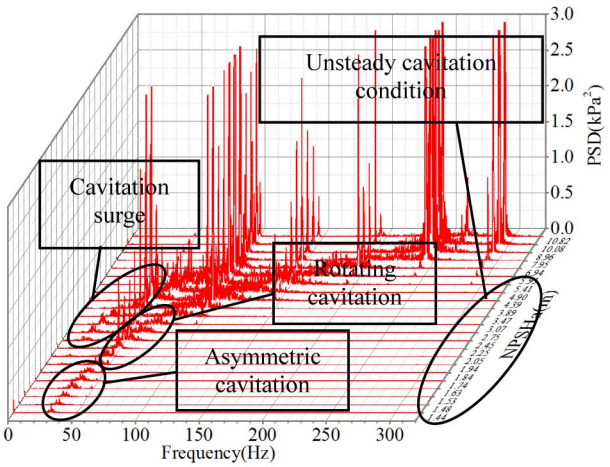

Fig. 5. Waterfall plot of pump inlet pressure pulsations at Q_d.

to 100 KPa and 0 to 0.6 MPa are respectively installed at the inlet and outlet of the pump to monitor the pressure pulsations. The inlet pressure and flow rate are adjusted by the vacuum pump and the flow control valve, respectively. The sampling rate of the pressure pulsations is 5000 Hz. The vibration signals are measured by the piezoelectric accelerometers whose type is MA352A60 with their ranges from 5 Hz to 70 kHz. The sampling frequency of the vibration signals is 20000 Hz. A PXI 4772B data acquisition module made by National Instruments Company is applied to capture the electric signals and convert them to digital signals. The test rig can meet the precision of national specifications of China. More detailed information about the pump can be obtained from the previous papers [27, 28].

4. Results and discussion

4.1 Unsteady cavitation

According to the previous research results [27, 28], reasonable agreements between the experimental and numerical results can be found from the performance with the variations of flow rate, and the suction performance curve of the pump with the wide ranges of pump inlet pressure. The results imply that this numerical method is feasible for the cavitating flow in the pump. The Power spectral density (PSD) signals of pump inlet pressure pulsations at Q_d is shown in Fig. 5. It can be found that during the cavitation progressing, not only the amplitude and the migration of dominant frequency of the PSD signals change apparently, but also the broadband pulsations are generating. Meanwhile, various types of cavitation instabilities in the centrifugal pump can be found. According to the research of Tsujimoto and Kimura et al. [14, 16, 25] and the research results which are discussed in the following parts in this paper, the unsteady cavitation occurs as the *NPSH*a decrease to about 5.93 m. While, the *NPSH*a decrease from 4.39 m to 1.44 m can be regarded as the unsteady cavitation became severe in the pump. It includes the process of Cavitation develops from Cavitation surge (CS), Rotating cavitation (RC) to Asymmetric cavitation (AC) in this pump. It can be regarded as the cavitation surge as the *NPSH*a decreases from 4.93 m to 2.25 m in this paper. Furthermore, it is considered that *NPSH*a decreases from 3.07 m to 1.84 m is the process of rotating cavitation. Therefore, cavitation surge and rotating cavitation are coexisted in part of the cavitation developing process. It may be certified through changing the length of the pump upstream and downstream pipe, and it inspires me to do further research to discern it. The asymmetric cavitation is apparently observed when *NPSH*a decreases from 1.74 m to 1.44 m through the numerical results. It is reported that vibration can be greatly induced by asymmetric cavitation [21]. The development of cavitation is also verified through the vibration signals induced by cavitation in this pump. It is reported that the positive mass flow gain factor is the cause of the instabilities for the condition of cavitation surge and rotating cavitation [29].

4.2 Internal flow characteristics of unsteady cavitation

Figs. 6 and 7 compare the distribution of water vapor volume fraction on the blades and in the axial plane at $b/b_2 = 0.1$ between non-cavitation and unsteady cavitation conditions at Q_d. Where b is the axial span between the interface of shroud and blades' outlet and the axial plane, and b_2 is the outlet width of the blades. As *NPSH*a decreases to 4.39 m, apparent uneven water vapor volume fraction distributes on the suction side of the leading edge is starting to generate. As the decrease of *NPSH*a, the length of the cavities on the blades which are close to the volute tongue is larger than that on the other blades. Evident asymmetry in the distribution of cavity volume can be found on the suction side of the blades in Fig. 6 when *NPSH*a decreases to 1.74 m. It can be observed that the vapor bubbles are propagating greatly to the downstream of the blade along the blades' suction side. At the same time, they are being produced on the pressure side of the blades which are next to the volute tongue while *NPSH*a reduces to 1.74 m in Fig. 7. As the further decreasing of *NPSH*a, the

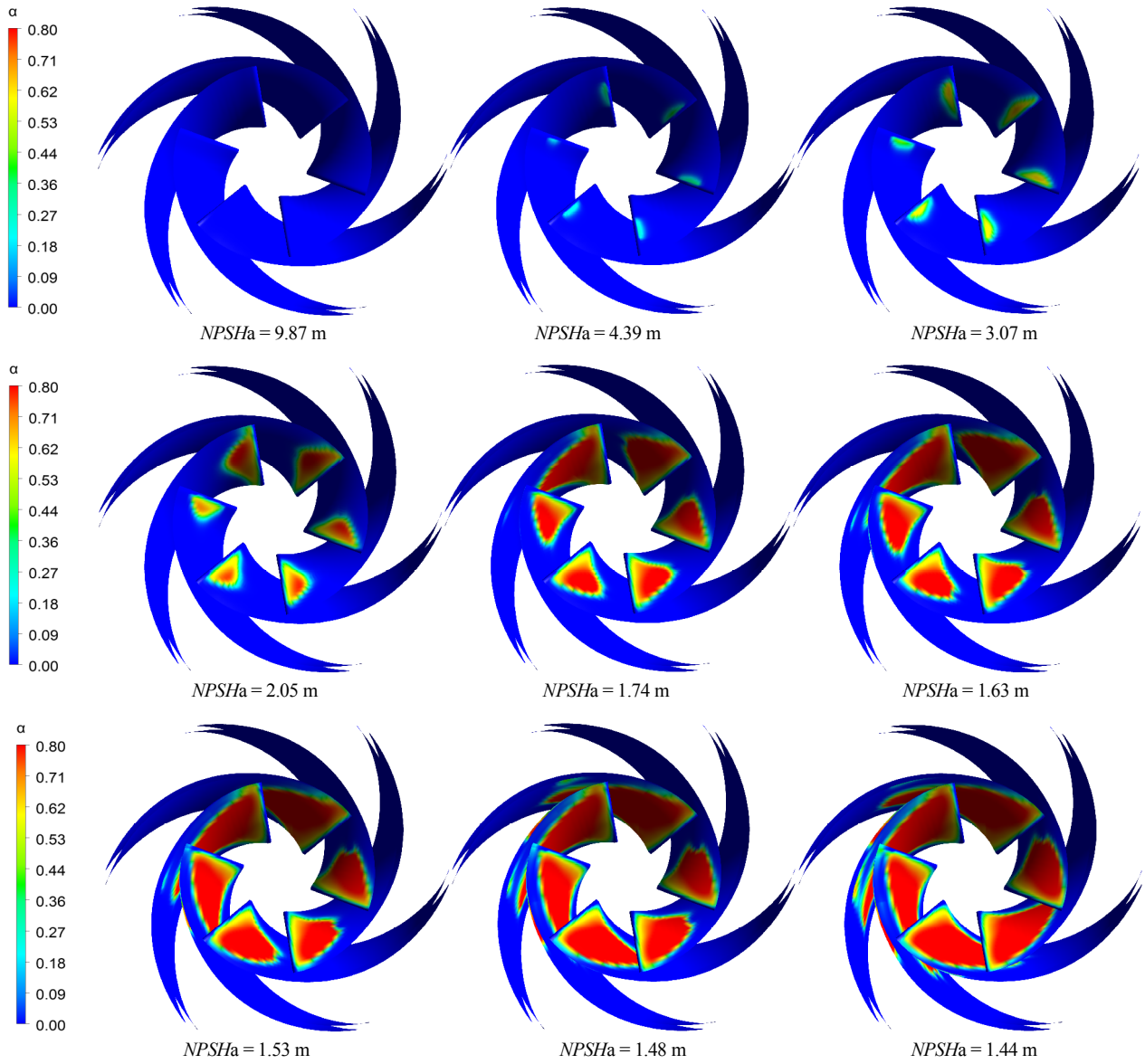

Fig. 6. Vapor volume fraction distribution on the blades at Q_d.

length of cavities quickly become larger and more uneven, and then the cavities rapidly propagate to the downstream of the channel along the suction surface of each blade. Obvious asymmetric and uneven distributions of vapor volume fraction are shown in each blade channel in Fig. 7. Owing to the interaction between the rotor and stator, the length of cavities is larger in these blade channels adjacent to the volute tongue than those are not closed to the tongue. However, as the further development of cavitation, cavities emerge and then diffuse to the downstream on the pressure surface of the blades' leading edge which are near the volute tongue. Asymmetric distribution of cavities on both sides of the blades' leading edge indicate that the cavitation has fully developed and the transformation from rotating cavitation to asymmetric cavitation is generating in the centrifugal pump. As the *NPSH*a decreases to 1.74 m, the asymmetric cavitation has been produced clearly in the leading edge of the blade which is adjacent to the volute tongue. While *NPSH*a decreases to 1.48 m, asymmetric distribution of cavitation can be found in the leading edge of the blades that are not close to the volute tongue, which are relatively weaker than those near the tongue. Asymmetric cavitation bubbles simultaneously distribute on both sides of the blade when *NPSH*a decreases to 1.53 m or lower, and then the length of the cavities becomes larger and propagates to the downstream. In this situation, the flow channels are choked by the generation of large cavitation bubbles, which lead to the efficiency and head drop sharply. It is considered that such uneven cavity volume distribution not only results from the rotor-stator interaction, but also the asymmetric distribution of cavity volume between each blade impacts with each other, which lead to asymmetric cavitation and other types of cavitation instabilities either.

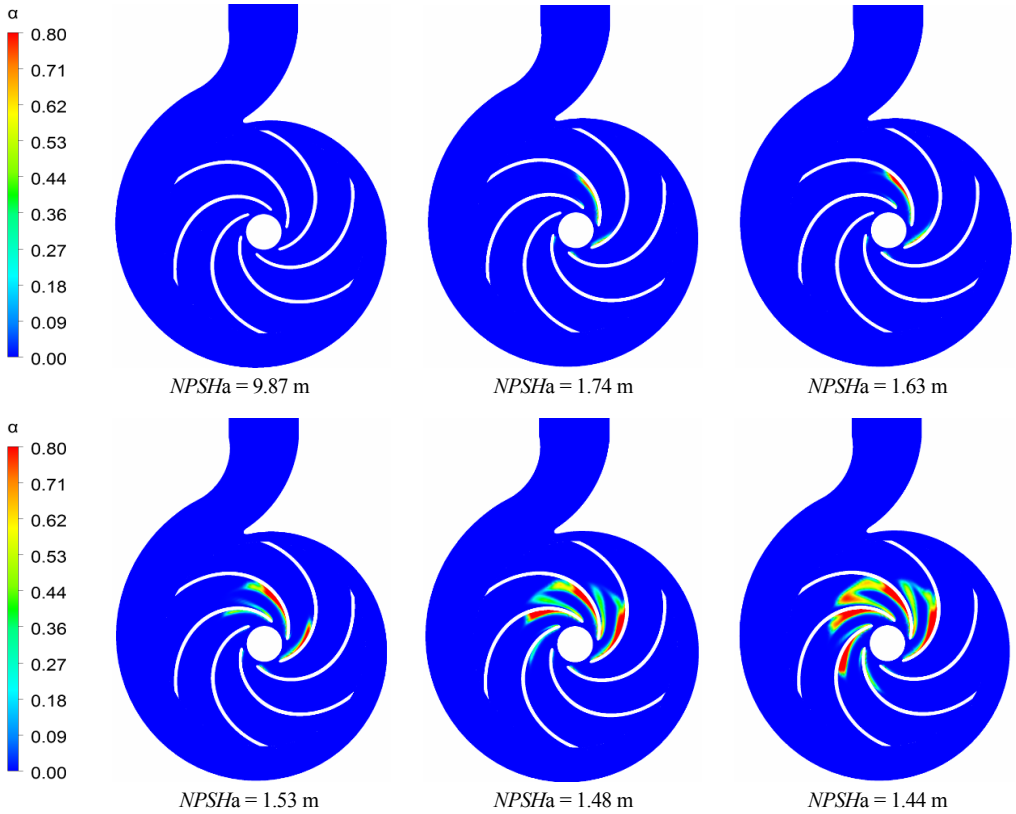

Fig. 7. The distribution of vapor volume fraction in axial plane at $b/b_2 = 0.1$, Q_d [30].

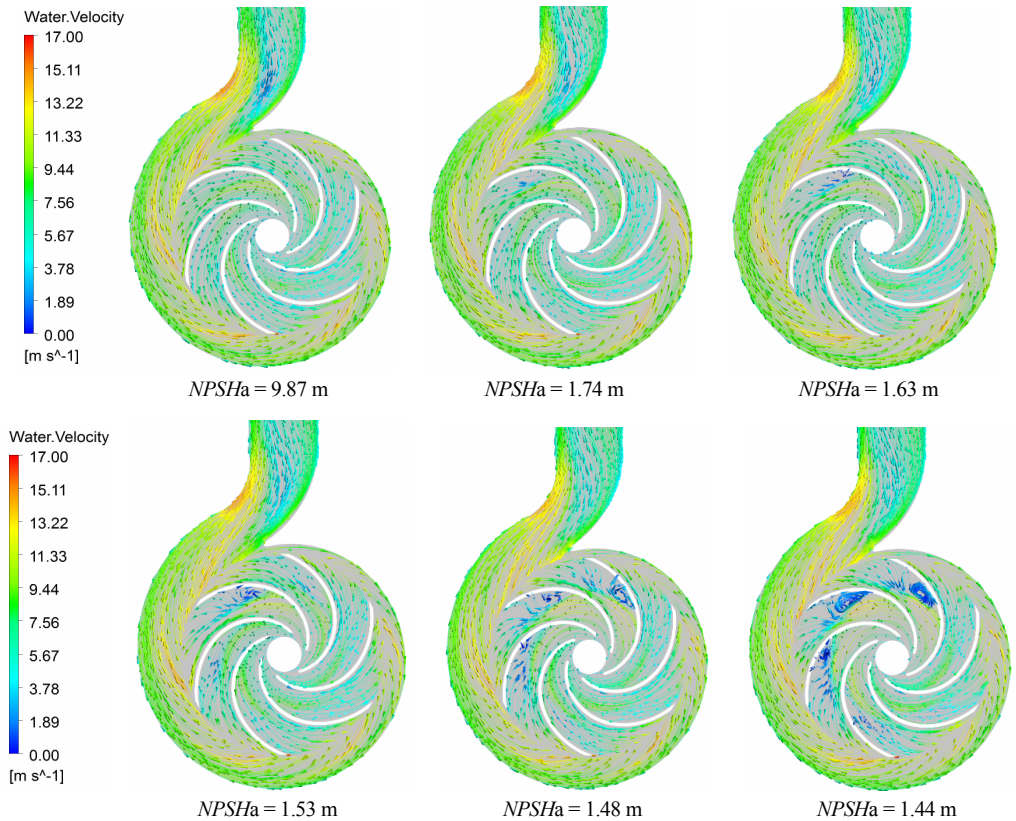

Fig. 8. Velocity distribution in axial plane at $b/b_2 = 0.1$, Q_d [30].

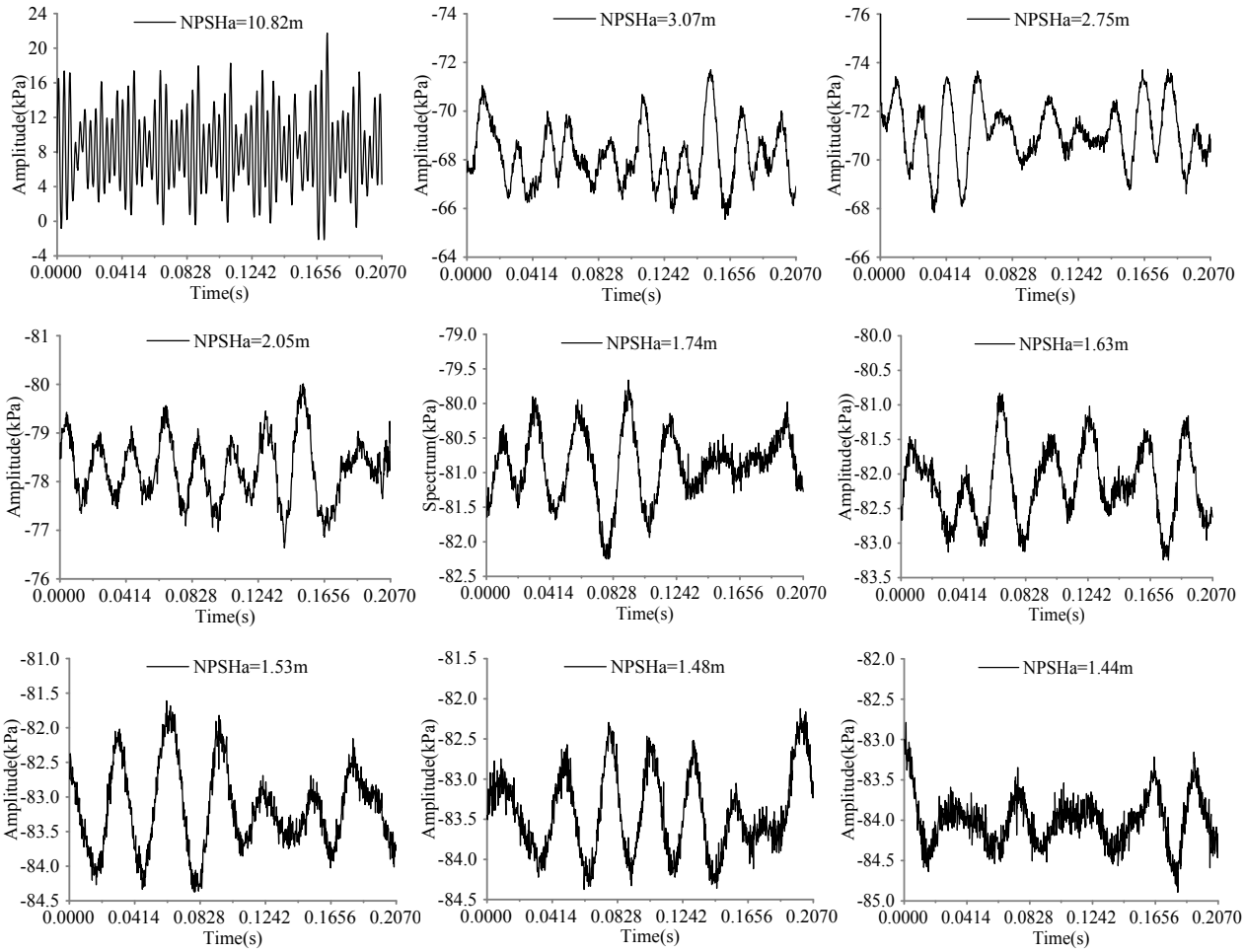

Fig. 9. Time domain signals of pump inlet pressure pulsations at Q_d.

The flow characteristics of velocity at Q_d in the axial plane at $b/b_2 = 0.1$ between non-cavitating condition, and the condition transition from rotating cavitation to asymmetric cavitation are compared in Fig. 8. It is found that the vortexes first appear in the leading edge of the blades' suction side which are next to the volute tongue. During the cavitation progressing, the vortexes become more apparent and the flow instabilities in the impeller intensified. With the further development of cavitation, the location of the vortexes expand to the blade passages which are not next to the volute tongue, and the rotating direction of the vortexes in each blade channel is consistent with the impeller rotating direction. Evident asymmetry and unevenness of vortex flow between each blade passage are seen. It is clear that a corresponding relationship between the distribution of cavity and the position of vortex in each blade channel is found. The positions of the vortexes' occurrence are in the cavity trailing edges. It is considered that the vapor bubbles shed, collapse and drive the spiral movement of the surrounding fluid. On the other hand, the high speed jets of surrounding fluid are produced by the sharp drop of the volume of the bubbles due to the collapse and condense of the cavitation bubbles, which lead to instabilities of vortexes in the collapse and shedding regions. The asymmetric flow between each blade channel also interferes with each other, impacting the incident angle of the adjacent passages, which will then aggravate the flow instabilities.

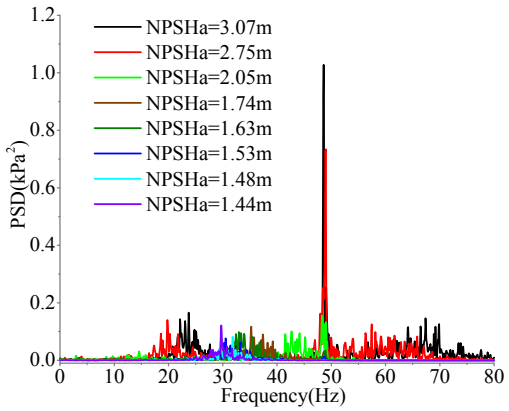

Fig. 10. Power spectral density of pump inlet pressure pulsations at Q_d.

4.3 Pump inlet pressure pulsations of unsteady cavitation

The characteristics of pump inlet pressure pulsations under the condition of unsteady cavitation at Q_d are analyzed

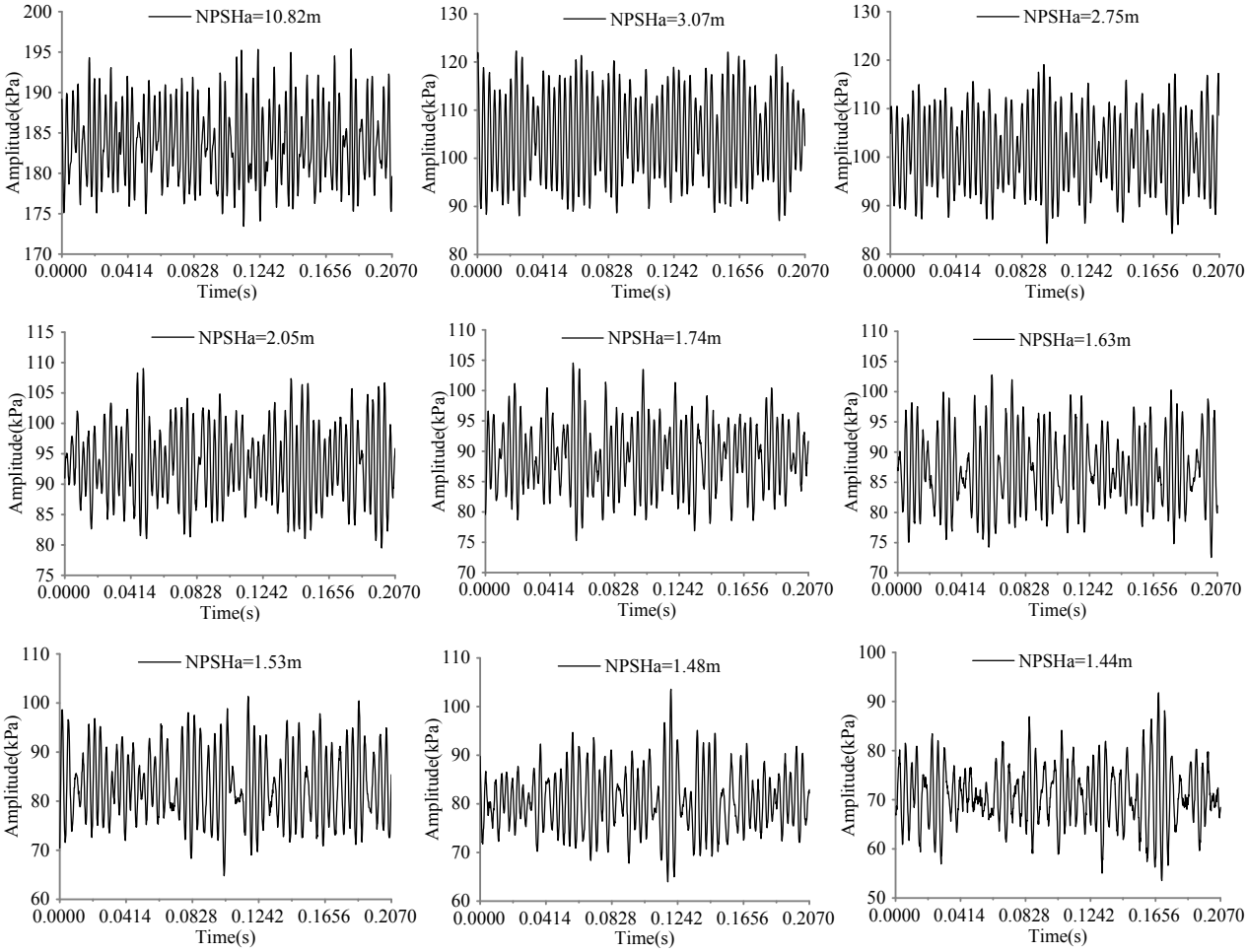

Fig. 11. Time domain signals of pump outlet pressure pulsations at Q_d.

through the time domain signals, shown in Fig. 9. The horizontal axis is the time that the impeller rotates 10 revolutions. The vertical axis shows the amplitude of pump inlet pressure pulsations under a certain specific value of *NPSH*a. It can be found that the pressure pulsations of pump inlet change from obvious periodic trends to irregular trends from non-cavitation condition to unsteady cavitation condition. Meanwhile, the ranges of the pulses' amplitude decrease greatly, and the fluctuation intensifies during the progressing of cavitation. The periods of the pump inlet pressure fluctuations become different which result from the random collapse and shedding of cavitating bubbles under the unsteady cavitation conditions. Fig. 10 shows the PSD signals of pump inlet pressure pulsations under the conditions of RC and AC at Q_d. It can be observed that the dominant frequency of the pump inlet pressure fluctuations is the shaft frequency, and the broadband pulsations of the pressure obviously distribute between 15 Hz to 30 Hz and 50 Hz to 80 Hz with the *NPSH*a reducing from 3.07 m to 2.05 m. Then, as the further decreasing of *NPSH*a, the dominant frequency of the pressure fluctuations moves to lower frequency bands and keeps at about 0.6-0.8 times (around 30-40 Hz) of the shaft frequency, and the amplitude is reduced greatly with severe fluctuating. The explanation for this phenomenon is that the flexible vapor bubbles' generation and combination with each other enhance the buffering effect to the pump inlet liquid. The collapse and shedding of cavitation bubbles mainly influence the pump inlet pressure fluctuations under the conditions that transform from RC to AC.

4.4 Pump outlet pressure pulsations of unsteady cavitation

Fig. 11 shows the time domain characteristics of pump outlet pressure pulsations at Q_d as the cavitation progressed. The abscissa represents the time of impeller rotating 10 revolutions and the ordinate is the amplitude of outlet pressure pulsations. It is found that compared to the non-cavitation condition, the variation of the pressure amplitude increases from about 20 kPa to 50 kPa, and the fluctuation intensifies as the cavitation develops from non-cavitation to unsteady cavitation. The ranges of the variation of the pump outlet pressure fluctuations' amplitude are much larger than that of the pump inlet pressure fluctuations under the unsteady cavitation conditions. However, the intensification of the pump inlet pressure fluctuation is more severe than that of the pressure which is tested

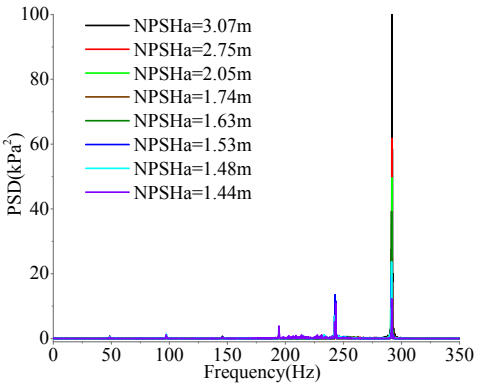

Fig. 12. Power spectral density of pump outlet pressure pulsations at Q_d.

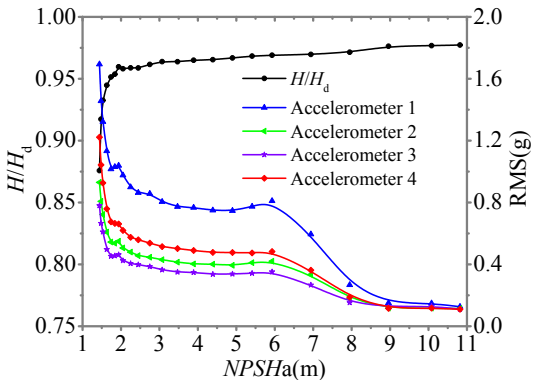

Fig. 13. Root mean square of vibration and the suction performance curve.

at the pump outlet. The explanation for this phenomenon is that not only the pressure at the pump inlet is much lower than that of the pump outlet, which is much easier to be affected by cavitation; but also the collapse and shedding of vapor bubbles are closer to the pump inlet than that of the pump outlet. Fig. 12 conveys the PSD signals of pump outlet pressure pulsations under the unsteady cavitation condition. The dominant frequency of the pressure pulsations is the blade passing frequency, which is approximately 290 Hz. Evident sub-peaks at shaft frequency and its octave frequency band are found. At the same time, the random generation, collapse and shedding of unsteady cavities between each blade channel result in the occurrence of broadband pulsations which distribute between 170 and 270 Hz. As the cavitation develops from RC to AC, the broadband pulsations become more severe. The maximum value of the PSD at the main frequency decreases sharply, but the PSD values at the other octave frequency increase when the cavitation fully develops.

4.5 The vibration signals of unsteady cavitation

Fig. 13 depicts the Root mean squares (RMS) of vibration in different positions and the suction performance curve of the pump. The calculation formula of RMS is shown in Eq. (1).

$$RMS = \sqrt{\frac{1}{N}\sum_{k=1}^{N} X_k^2} \tag{1}$$

where X_k represents the value of the vibration measured at some moment. k = 1, 2, 3,…, *N*. It can be found that the RMS of vibration and the head of the pump change obviously with the development of cavitation. According to the RMS signals of the vibration measured by the four accelerometers, similar developmental trends are found during the cavitation progressing. The RMS of the vibration signals measured in different positions are almost the same under the non-cavitation condition with the *NPSH*a decrease from 10.82 m to 8.96 m. The RMS signals start to increase and the head begins to drop as the *NPSH*a decreases to 7.95 m. Then the RMS signals keep a relatively steady state with the *NPSH*a reducing from 5.93 m to 4.39 m. After that the RMS signals rise up again, which also indicates that the cavitation instabilities became more severe at that point. While *NPSH*a decreases to 3.07 m, the RMS signals of vibration increase quickly in the four different positions. As the further development of cavitation, the RMS signals of vibration sharply increase while *NPSH*a decreases to 1.74 m; at the same time, the head of the pump drops dramatically. The explanation for this phenomenon is that the increasing of RMS of vibration is induced by the development of cavitation. With the decreasing of the pump inlet pressure, the incipient cavitation occurs when the *NPSH*a decreases to 7.95 m, which produces the beginning increase of the vibration and the decrease of the head. This results shows that the point of cavitation occurs is greater than that of the previous research which was detected by the pump inlet and outlet pressure pulsations. Then quasi-steady cavitation has been generated before *NPSH*a decreases to 5.93 m, and the RMS signals of vibration keep a relatively steady state until the *NPSH*a reduces to 3.07 m. While *NPSH*a decreases to 1.94 m, cavity volume increase quickly which extrude the liquid and make the liquid get more energy. As a result, the head increases at this moment. Meanwhile, the instabilities become more sever which strengthen the vibration. As the further decrease of *NPSH*a, the expanding cavitation bubbles occupy a large part of passage and obstruct the liquid into the impeller, which induce the sharp increase of vibration and dramatic drop in head. It is observed that the value of the RMS of the vibration tested by accelerometer 1 is larger than that of the other accelerometers. The reason for this phenomenon is that the position of accelerometer 1 is closer to the impeller and the generation of cavitation than that of other accelerometers, which collects the strongest vibrating signals. Then, the RMS of the vibration tested by accelerometer 4 is stronger than that of accelerometers 2 and 3. The primary reason is that accelerometer 4 is installed on the foundation of the pump system, which gathers not only the vibration induced by cavitation, but also the vibration produced by the whole mechanical system. It also demonstrates that cavitation plays a dominant role to the vibration compared to the mechanical system under the unsteady cavitation condition. The RMS signals of the vibra-

tion climb up drastically, which corresponds to the sharp drop in head of the pump from the occurrence of the asymmetric cavitation. Therefore, it is significant to prevent a pump operating under the unsteady cavitation conditions.

5. Conclusions

The internal flow in the impeller, the pump inlet and outlet pressure pulsations, and the vibration in different positions under the unsteady cavitation conditions have been investigated through numerical simulation and experimental method in a centrifugal pump. It can be found that the unsteady cavitation starts to occur as the *NPSH*a is lower than 5.93 m. Asymmetric and uneven cavity volume distributions on each blade and the impeller are observed apparently as the *NPSH*a decreases from 4.39 m to 1.44 m which includes the cavitation develops from cavitation surge, rotating cavitation to asymmetric cavitation. The flow vortexes in each blade channel are produced in the cavity trailing edges by the shedding and collapse of cavitation, which interfere with each other and aggravate the flow instabilities. The dominant frequencies of the pump inlet and out pressure fluctuations are the shaft frequency and blade passing frequency under the unsteady cavitation conditions, respectively. Some broadband pulses are found from both the pump inlet and outlet pressure pulsations, which results from the random shedding and collapse of cavitation bubbles. Obvious corresponding relationship between the Root mean squares (RMS) of the vibration tested in different positions and the suction performance curve is obtained under both the non-cavitation condition and unsteady cavitation condition. This work provides a good reference for the unsteady cavitation research and the cavitation detection in centrifugal pumps.

Acknowledgments

This research was supported by the State Key Program of National Natural Science Foundation of China (Grant No. 51239005), the Program of National Natural Science Foundation of China (Grant No.51479082 & 51509108), the project supported by the Science & Technology Promotion Plan of Ministry of Water Resources of China (Grant No. TG1521), and the Priority Academic Program Development of Jiangsu Higher Education Institutions (PAPD).

Nomenclature

b : Axial span between the interaction of shroud and blade outlet and the axial plane
b_2 : Outlet width of blade
f_d : Blade passing frequency
f_0 : Shaft frequency
H_d : Designed pump head
*NPSH*a : $(p_{inlet}-p_v)/\rho g$, available net positive suction head
*NPSH*r : Required net positive suction head
n_s : $3.65\ nQ^{0.5}/H^{0.75}$, specific speed
p_{inlet} : Pressure at pump inlet
p_v : Vapor pressure
PSD : Power spectral density
Q_d : Designed flow rate
RMS : Root mean squares
X_k : The value of the vibration
ρ : Density of water

References

[1] S. Christopher and S. Kumaraswamy, Identification of critical net positive suction head from noise and vibration in a radial flow pump for different leading edge profiles of the vane, *Journal of Fluids Engineering*, 135 (12) (2013) 121301.

[2] X. Yu, C. Huang, T. Du, L. Liao, X. Wu, Z. Zheng and Y. Wang, Study of characteristics of cloud cavity around axisymmetric projectile by large eddy simulation, *Journal of Fluids Engineering*, 136 (5) (2014) 051303.

[3] X. Luo, B. Ji and Y. Tsujimoto, A review of cavitation in hydraulic machinery, *Journal of Hydrodynamics*, *Ser. B*, 28 (3) (2016) 335-358.

[4] Y. Ni, S. Yuan, Z. Pan and J. Yuan, Detection of cavitation of in centrifugal pump by vibration methods, *Chinese Journal of Mechanical Engineering*, 21 (5) (2008) 46-49.

[5] M. Chudina, Noise as an indicator of cavitation in a centrifugal pump, *Acoustical Physics*, 49 (4) (2003) 463-474.

[6] J. Cernetic, The use of noise and vibration signals for detecting cavitation in kinetic pumps, *Journal of Mechanical Engineering Science*, 223 (7) (2009) 1645-1655.

[7] Y. Su, Y. Wang and X. Duan, Cavitation experimental research on centrifugal pump, *Transactions of the Chinese Society for Agricultural Machinery*, 41 (3) (2010) 77-80.

[8] H. Horiguchi, S. Watanabe and Y. Tsujimoto, A linear stability analysis of cavitation in a finite blade count impeller, *Journal of Fluids Engineering*, 122 (4) (2000) 798-805.

[9] H. Horiguchi, S. Watanabe, Y. Tsujimoto and M. Aoki, A theoretical analysis of alternate blade cavitation in inducers, *Journal of Fluids Engineering*, 122 (1) (2000) 156-163.

[10] Y. Semenov, A. Fujii and Y. Tsujimoto, Rotating choke in cavitating turbopump inducer, *Journal of Fluids Engineering,* 126 (1) (2004) 87-93.

[11] X. Peng, B. Ji, Y. Cao, L. Xu, G. Zhang, X. Luo and X. Long, Combined experimental observation and numerical simulation of the cloud cavitation with U-type flow structures on hydrofoils, *International Journal of Multiphase Flow*, 79 (2016) 10-22.

[12] D. Kang, K. Yonezawa, H. Horiguchi, Y. Kawata and Y. Tsujimoto, Cause of cavitation instabilities in three dimensional inducer, *International Journal of Fluid Machinery and Systems*, 2 (3) (2009) 206-214.

[13] R. Balasubramanian, S. Bradshaw and E. Sabini, Influence of impeller leading edge profiles on cavitation and suction performance, *Proceedings of the 27th International Pump*

Users Symposium (2011) 12-15.

[14] J. Fredrichs and G. Kosna, Rotating cavitation in a centrifugal pump impeller of low specific speed, *Journal of Fluids Engineering*, 124 (2) (2002) 356-362.

[15] J. Lu, S. Yuan, X. Li, Q. Si and Y. Luo, Research on the characteristics of quasi-steady cavitation in a centrifugal pump, *IOP Conference Series: Materials Science and Engineering*, 72 (3) (2015) 032017.

[16] T. Kimura, Y. Yoshida, T. Hashimoto and M. Shimagaki, Numerical simulation for vortex structure in a turbopump inducer: Close relationship with appearance of cavitation instabilities, *Journal of Fluids Engineering,* 130 (5) (2008) 051104.

[17] M. Subbaraman and K. Burton, Cavitation-induced vibrations in turbomachinery: Water-model exploration, *Proceedings of International Cavitation Symposium*, Osaka, Japan (2003).

[18] Y. Tsujimoto, Y. Yoshida, Y. Maekawa, S. Watanabe and T. Hashimoto, Observations of oscillating cavitation of an inducer, *Journal of Fluids Engineering,* 119 (4) (1997) 775-781.

[19] K. Kamijo, T. Shimura and M. Watanabe, An experimental investigation of cavitating inducer instability, *ASME paper*, 77 (1977).

[20] Y. Yoshida, M. Eguchi, T. Motomura, M. Uchiumi, H. Kure and Y. Maruta, Rotordynamic forces acting on three-bladed inducer under supersynchronous/synchronous rotating cavitation, *Journal of Fluids Engineering*, 132 (6) (2010) 061105.

[21] Y. Yoshida, Y. Kazami, K. Nagaura, M. Shimagaki, Y. Iga and T. Ikohagi, Interaction between uneven cavity length and shaft vibration at the inception of synchronous rotating cavitation, *International Journal of Rotating Machinery*, 2008 (2008) 218978.

[22] A. Fujii, S. Azuma, M. Uchiumi, Y. Yoshida and Y. Tsujimoto, Unsteady behavior of asymmetric cavitation in a 3-bladed inducer, *The Fifth International Symposium on Cavitation (Cav2003)*, Osaka, Japan (2003) 1-4.

[23] Y. Yoshida, H. Nanri, K. Kikuta, Y. Kazami, Y. Iga and T. Ikohagi, Thermodynamic effect on subsynchronous rotating cavitation and surge mode oscillation in a space inducer, *Journal of Fluids Engineering,* 133 (6) (2011) 061301.

[24] B. Ji, J. Wang, X. Luo, K. Miyagawa, L. Xiao, X. Long and Y. Tsujimoto, Numerical simulation of cavitation surge and vortical flows in a diffuser with swirling flow, *Journal of Mechanical Science and Technology*, 30 (6) (2016) 2507-2514.

[25] N. Tani, N. Yamanishi and Y. Tsujimoto, Influence of flow coefficient and flow structure on rotational cavitation in inducer, *Journal of Fluids Engineering,* 134 (2) (2012) 021302.

[26] Y. Tsujimoto, S. Watanabe and H. Horiguchi, Cavitation instabilities of hydrofoils and cascades, *International Journal of Fluid Machinery and Systems*, 1 (1) (2008) 38-46.

[27] J. Lu, S. Yuan, Y. Luo, J. Yuan, B. Zhou and H. Sun, Numerical and experimental investigation on the development of cavitation in a centrifugal pump, *Proceedings of the Institution of Mechanical Engineers, Part E: Journal of Process Mechanical Engineering*, 230 (3) (2016) 171-182.

[28] J. Lu, S. Yuan, X. Ren, Y. Liu and Q. Si, Investigation of instabilities of cavitation at low flow rate of centrifugal pump, *Transaction of the Chinese Society for Agricultural Machinery*, 46 (8) (2015) 54-58.

[29] Y. Tsujimoto, H. Horiguchi and K. Yonezawa, Cavitation instabilities in turbopump inducers, *International Journal of Fluid Machinery and Systems*, 3 (2) (2010) 170-180.

[30] J. Lu, S. Yuan, B. Zhou, Y. Luo and J. Yuan, Research on the characteristics under the condition of asymmetric cavitation in a centrifugal pump, *Fluid Machinery and Fluid Engineering, The ISFMFE-6th International Symposium on IET* (2014) 1-8.

Jiaxing Lu is currently a Ph.D. candidate in the National Research Center of Pumps, Jiangsu University. His research interests include the cavitation instabilities and analysis of unsteady flow of centrifugal pump. He received his B.S. degree from Xihua University in 2007.

Shouqi Yuan is currently a Professor in the National Research Center of Pumps, Jiangsu University. His research interests include the theory, optimization, and design of fluid machinery. He received his Ph.D. degree from Jiangsu University in 1994.